Research Article

Role of microtubule dynamics in Wallerian degeneration and nerve regeneration after peripheral nerve injury

https://doi.org10.4103/1673-5374.320997

Date of submission: February 3, 2021

Date of decision: April 25, 2021

Date of acceptance: May 31, 2021

Date of web publication: August 4, 2021

Jingmin Liu[1, 2], Lixia Li[1, 2], Ying Zou[1, 2], Lanya Fu[1, 2], Xinrui Ma[1, 2], Haowen Zhang[1, 2], Yizhou Xu[1, 2, 3], Jiawei Xu[1, 2], Jiaqi Zhang[1, 2], Mi Li[1, 2], Xiaofang Hu[1, 2], Zhenlin Li[1, 2], Xianghai Wang[1, 2, 4], Hao Sun[4], Hui Zheng[4], Lixin Zhu[3], Jiasong Guo[1, 2, 3, 4, 5, *]

Graphical Abstract

Regulating microtubule dynamics by paclitaxel or nocodazole can affect Wallerian degeneration and nerve regeneration after peripheral nerve injury

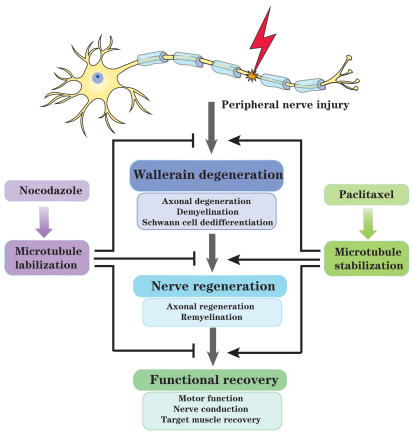

Abstract

Wallerian degeneration, the progressive disintegration of distal axons and myelin that occurs after peripheral nerve injury, is essential for creating a permissive microenvironment for nerve regeneration, and involves cytoskeletal reconstruction. However, it is unclear whether microtubule dynamics play a role in this process. To address this, we treated cultured sciatic nerve explants, an *in vitro* model of Wallerian degeneration, with the microtubule-targeting agents paclitaxel and nocodazole. We found that paclitaxel-induced microtubule stabilization promoted axon and myelin degeneration and Schwann cell dedifferentiation, whereas nocodazole-induced microtubule destabilization inhibited these processes. Evaluation of an *in vivo* model of peripheral nerve injury showed that treatment with paclitaxel or nocodazole accelerated or attenuated axonal regeneration, as well as functional recovery of nerve conduction and target muscle and motor behavior, respectively. These results suggest that microtubule dynamics participate in peripheral nerve regeneration after injury by affecting Wallerian degeneration. This study was approved by the Animal Care and Use Committee of Southern Medical University, China (approval No. SMU-L2015081) on October 15, 2015.

Key Words: axon; demyelination; microtubule dynamics; nerve regeneration; nocodazole; paclitaxel; peripheral nerve injury; Schwann cell; Wallerian degeneration

Chinese Library Classification No. R446; R745; Q245

Introduction

Wallerian degeneration (WD) is a progressive process of demyelination and anterograde disintegration of the distal axonal segment following transection of the axon, which may occur in peripheral nerve injury (PNI) or traumatic brain injury (Conforti et al., 2014). During WD, debris from degraded axons and myelin is removed by macrophages and Schwann cells to ensure a permissive microenvironment for axonal regeneration (Nocera and Jacob, 2020; Qu et al., 2021). Therefore, gaining a better understanding of WD could be helpful in developing novel therapeutic strategies for PNI. The morphology of axons and the myelin sheath changes

[1]Department of Histology and Embryology, School of Basic Medical Sciences, Southern Medical University, Guangzhou, Guangdong Province, China; [2]Guangdong Provincial Key Laboratory of Construction and Detection in Tissue Engineering, Southern Medical University, Guangzhou, Guangdong Province, China; [3]Department of Spine Orthopedics, Zhujiang Hospital of Southern Medical University, Guangzhou, Guangdong Province, China; [4]Bioland Laboratory (Guangzhou Regenerative Medicine and Health Guangdong Laboratory), Guangzhou, Guangdong Province, China; [5]Key Laboratory of Mental Health of the Ministry of Education, Guangdong-Hong Kong-Macao Greater Bay Area Center for Brain Science and Brain-Inspired Intelligence, Guangdong Province Key Laboratory of Psychiatric Disorders, Guangzhou, Guangdong Province, China

*__Correspondence to:__ Jiasong Guo, PhD, jiasongguo@smu.edu.cn.

https://orcid.org/0000-0002-7885-2903 (Jiasong Guo)

Funding: *This work was supported by the National Natural Science Foundation of China, Nos. 82071386 (to JS), 81870982 (to JS) & 81571182 (to JS); the National Key Basic Research Program of China, No. 2014CB542202 (to JS); the Program for Changjiang Scholars and Innovative Research Team in University of China, No. IRT-16R37 (to JS); Key Research & Development Program of Guangzhou Regenerative Medicine and Health Guangdong Laboratory of China, No. 2018GZR110104008 (to HZ); Research Grant of Guangdong Province Key Laboratory of Psychiatric Disorders of China, No. N201904 (to JS); and Natural Science Foundation of Guangdong Province of China, No. 2017A030312009 (to JS).*

How to cite this article: *Liu J, Li L, Zou Y, Fu L, Ma X, Zhang H, Xu Y, Xu J, Zhang J, Li M, Hu X, Li Z, Wang X, Sun H, Zheng H, Zhu L, Guo J (2022) Role of microtubule dynamics in Wallerian degeneration and nerve regeneration after peripheral nerve injury. Neural Regen Res 17(3):673-681.*

dramatically during WD, suggesting that the cytoskeleton, which includes microfilaments, intermediate filaments, and microtubules, is involved in this process. Indeed, the roles that microfilaments and intermediate filaments play in WD are well-established (Triolo et al., 2012; Wang et al., 2018). However, the relationship between microtubules and WD remains unclear.

Microtubules are intrinsically dynamic polymers. They have two states: stable and labile. The continuous transition between stable and labile states is called microtubule dynamics (Fees and Moore, 2018; Manka and Moores, 2018; Honoré et al., 2019). Microtubule dynamics are a key regulator of various biological activities (Maciel et al., 2018). For example, microtubule-targeting agents are widely used to treat cancer (Senese et al., 2017; Roviello et al., 2019). As axon regeneration may involve internal protrusive forces generated by microtubules, these agents are also considered to be potential therapies for central nervous system injury. Many studies have demonstrated that treatment with paclitaxel, a microtubule stabilizer, can promote central nervous system axonal regeneration (Hellal et al., 2011; Sengottuvel et al., 2011; Austin et al., 2017). In contrast, treatment with the microtubule-destabilizing agent nocodazole inhibits axonal regeneration in the central nervous system (Hu et al., 2018). However, little is known about the relationship between microtubule dynamics and peripheral nerve regeneration, and it remains unclear whether microtubule-destabilizing agents affect WD and nerve regeneration after PNI. While a few studies have investigated the effects of microtubule-stabilizing agents on PNI, the results are contradictory. For example, Hsu et al. (2017) reported that paclitaxel impairs nerve regeneration in a rat model of sciatic nerve transection, while Zhou et al. (2020) found that epothilone B, another U.S. Food and Drug Administration–approved microtubule-stabilizing agent, facilitates peripheral nerve regeneration. To our knowledge, the current study is the first to describe the role of microtubule dynamics in WD, and the first to explore the effects of both a microtubule-stabilizing agent (paclitaxel) and a microtubule-destabilizing agent (nocodazole) on PNI repair.

Materials and Methods

Experimental animals and ethics statement

Twenty-seven specific pathogen-free Sprague-Dawley female adult rats (aged 8 weeks) weighing 200–250 g and five neonatal rats (postnatal day 3) were provided by the Animal Center of Southern Medical University, China (license No. SCXK (Yue) 2016-0041). The rats were housed in an animal room maintained at 21°C and 55% relative humidity with a 12-hour light/dark cycle and given free access to water and food. All procedures, including surgery and tissue collection, were carried out with the approval of the Southern Medical University Animal Care and Use Committee (approval No. SMU-L2015081, approval date October 15, 2015) in accordance with the guidelines for the ethical treatments of animals. All efforts were made to minimize the number of animals used and their suffering.

Sciatic nerve explant culturing and treatment

Sciatic nerve explant culturing, which is an *in vitro* model of WD, was performed as described previously (Shin et al., 2013; Park et al., 2015; Li et al., 2021). Briefly, nine adult rats were anesthetized by intraperitoneal injection of 12 mg/mL tribromoethanol (180 mg/kg; Sigma-Aldrich, St. Louis, MO, USA) and decapitated by guillotine. Sciatic nerve segments (0.5 cm in length) were isolated and incubated in the Dulbecco's modified Eagle's medium/F12 (Corning, New York, NY, USA) containing 3% fetal bovine serum (Corning), 3 mM forskolin (Sigma-Aldrich), 10 ng/mL heregulin (PeproTech, Rocky Hill, NJ, USA), and 100 mg/mL penicillin-streptomycin (Gibco, Grand Island, NY, USA). Paclitaxel (Sigma-Aldrich) or nocodazole (Sigma-Aldrich) was dissolved in anhydrous dimethyl sulfoxide (Sigma-Aldrich) to produce a 2 or 10 mg/mL stock solution, respectively, which was stored at –20°C until administration. Paclitaxel or nocodazole was added to the culture medium, and the nerve explants were collected after culturing for 5 or 8 days *in vitro* (div) for subsequent analysis. A vehicle-only control group was included.

Schwann cell culturing and treatment

The concentrations of paclitaxel and nocodazole to be used for subsequent experiments were determined based on a previous report (Imai et al., 2017) and preliminary experiments performed using cultured Schwann cells. First, Schwann cells were isolated from neonatal rats as we described earlier (Wen et al., 2017, 2018; Tan et al., 2018). Briefly, five neonatal rats were subjected to hypothermic anesthesia by placing them on ice, and then disinfected with 75% alcohol. Next, all the spinal nerves were aseptically isolated and digested with 0.25% Trypsin-ethylene diamine tetraacetic acid (Gibco) to obtain a single-cell suspension. After incubation in Dulbecco's modified Eagle's medium/F12 containing 10% fetal bovine serum in poly-L-lysine (Sigma-Aldrich)-coated petri dish (Jet Biofil, Guangzhou, China) for 24 hours, the cells were treated with 10 μM of cytosine arabinoside (Sigma-Aldrich) for 48 hours to eliminate the fibroblasts. Subsequently, the cells were cultured in the Dulbecco's modified Eagle's medium/F12 containing 3% fetal bovine serum, 3 μM forskolin (Sigma-Aldrich), and 10 ng/mL heregulin (PeproTech). The passage 3 cells were then treated with paclitaxel (1, 10, 50, 100, or 200 nM) or nocodazole (1, 10, 100, 500, or 1000 nM) for 24 hours. Morphologic changes were observed with a phase contrast microscope (Leica, Wetzlar, Germany) immediately after treatment, or after an additional 24 hours of culturing in fresh medium to assess washout effects (Felitsyn et al., 2007).

Sciatic nerve crush injury model and treatment

A rat model of sciatic nerve crush injury was established as described previously (Qian et al., 2018). Briefly, adult rats were randomly divided into vehicle, paclitaxel, and nocodazole groups (n = 6 for each group) and anesthetized by intraperitoneal injection of 180 mg/kg tribromoethanol. Then, the bilateral sciatic nerves were bluntly exposed, and a crush injury 0.5 cm distal to the sciatic notch was performed by clamping the nerve with a smooth, straight hemostat (tip width 2 mm) for 2 minutes. Before the incision was closed, the crush site was marked with a 9-0 nylon suture. Immediately after the surgery, rats were injected intraperitoneally with 100 μL paclitaxel (200 μM, stock solution diluted with saline), nocodazole (1000 μM, stock solution diluted with saline), or vehicle (dimethyl sulfoxide diluted with saline), as described previously (Cook et al., 2018). At 3 days post injury (dpi), three rats from each group were anesthetized by intraperitoneal injection of 180 mg/kg tribromoethanol, after which the left sciatic nerves were collected for western blot assay. Next, transcardial perfusion with 4% paraformaldehyde was performed, and the right sciatic nerves were collected for immunohistochemistry. The remaining three rats in each group were treated with the appropriate drug (or control injection) every 2 days for 2 weeks following the surgery. At 28 dpi, behavioral assessments and electrophysiological tests were performed, after which the rats were sacrificed and tissues were collected for further assays (**Additional Figure 1**).

Behavioral assessment and electrophysiological testing

Recovery of motor function controlled by the injured sciatic nerve was detected using a catwalk analysis system (DigiGait, Framingham, MA, USA) (Glajch et al., 2012). From 25 to 27 dpi, the rats were trained to walk on the motorized transparent treadmill belt three times per day. At 28 dpi, their footprints were captured using a video camera set beneath the belt to calculate the sciatic functional index (SFI) using the associated

software (Wu et al., 2011). The SFI was calculated according to the following formula: SFI = –38.3(EPL– NPL)/NPL + 109.5(ETS – NTS)/NTS + 13.3(EIT– NIT)/NIT – 8.8. Three different parameters were measured: (1) distance from the heel to the third toe (print length; PL); (2) distance from the first toe to the fifth toe (toe spread; TS); and (3) distance from the second toe to the fourth toe (intermediate toe spread; ITS); E indicates experimental animals, and N indicates normal animals.

Six hours after the final behavioral test, the rats were anesthetized with 180 mg/kg tribromoethanol, and electrophysiological testing was performed (Pan et al., 2017; Li et al., 2019; Hu et al., 2020; Lai et al., 2020). Briefly, a pair of needle electrodes was inserted to stimulate the sciatic nerve 3 mm proximal to the crush site, and a pair of recording electrodes was inserted subcutaneously into the middle of the intrinsic foot muscle. After a single stimulation with a strength of 10 mA and a duration of 0.1 ms, the amplitude and latency of the compound muscle action potential (CMAP) were recorded with a set of electrophysiological recorders (frequency of 20 Hz and pulse width of 0.1 ms) (Axon Digidata 1550 Digitizer, Molecular Devices, Sunnyvale, CA, USA). Immediately after the CMAP recording, the rats were transcardially perfused, and the gastrocnemius muscles and sciatic nerves were collected for the following assessments.

Histomorphometry of the gastrocnemius muscle

To assay the level of myoatrophy of the target muscle of the injured nerve, the wet weight of the bilateral gastrocnemius muscles collected at 28 dpi was measured on a laboratory scale (METTLER TOLEDO, Zurich, Switzerland). Then the mid-belly of the muscles was trimmed for routine paraffin embedding, transversal sectioning, and hematoxylin-eosin staining to visualize the myofibers. As described previously (Wang et al., 2014; Pan et al., 2017), six non-overlapping images of every eighth section from each animal were captured, and the total myofiber area was quantified using Image-Pro Plus 6.0 software (Media Cybernetics, Silver Spring, MD, USA).

Immunohistochemistry of cryosections and teased nerve fibers

The distal trunk of the injured sciatic nerve was harvested from the perfused rats at 3 or 28 dpi, and the nerve explants were collected at 5 or 8 div. Both types of nerve segments were fixed in 4% paraformaldehyde for 24 hours and dehydrated in 30% sucrose overnight. Then they were embedded in optimal cutting temperature compound (Sakura Finetek, Torrance CA, USA) for cryosectioning and subsequent immunofluorescence staining. To assess the myelin ovoid formation that occurs during WD, five nerve explants from each group were also teased into individual fibers and mounted on adhesion slides (Guo et al., 2014; Wen et al., 2017).

The 10 μm-thick cryosection slices and teased fibers were stained for immunohistochemistry as follows. The samples were first permeabilized with 0.5% Triton X-100 (Sigma) for 30 minutes, then blocked with 5% fish gelatin (Sigma) containing 0.3% Triton X-100 at room temperature for 1 hour, followed by incubation with the primary antibodies diluted in blocking buffer overnight at 4°C. Goat anti-rabbit Alexa Fluor 488 (1:400, Cat# A-11008), goat anti-rabbit Alexa Fluor 568 (1:400, Cat# A-11011), and goat anti-mouse Alexa Fluor 568 (1:400, Cat# A-11031) fluorescent-conjugated secondary antibodies (all from Molecular Probes, Eugene, OR, USA) were applied for 2 hours at room temperature. The samples were then incubated with 4′,6-diamidino-2-phenylindole (1:5000; Sigma) for 2 minutes to counterstain the cell nuclei. Finally, images were captured using a fluorescence microscope (Leica). The primary antibodies used for immunocytochemistry were as follows: mouse anti-myelin basic protein (MBP; 1:200, Cat# NE1018, Calbiochem, Darmstadt, Germany), rabbit anti-neurofilament 200 (NF200; 1:400, Cat# N0142, Sigma), mouse anti-α-tubulin (1:1000; Cat# AB7291, Abcam, Cambridge, UK), rabbit anti-myelin-associated glycoprotein (MAG; 1:400; Cat# AB89780, Abcam), mouse anti-c-Jun (1:400; Cat# 610326, BD Biosciences, New York, NY, USA), rabbit anti-growth-associated protein 43 (GAP43; 1:400, Cat# ab16053, Abcam), and rabbit anti-superior cervical ganglia protein 10 (SCG10; 1:500; Cat# NBP1–49461, Novusbio, Littleton, CO, USA).

Oil red O staining

To assess myelin degradation during WD, oil red O (ORO) staining was performed on the nerve explant cryosection (Li et al., 2021). Briefly, the 0.3% ORO staining solution was prepared by mixing ORO (dissolved in 60% 2-propanol) with deionized water (ratio = 3:2). The sections were rinsed in 0.01 M phosphate buffered saline and 60% isopropanol, then incubated in the ORO solution for 15 minutes at 37°C and rinsed in 60% isopropanol and 0.01 M phosphate buffered saline and mounted. Images of each section were captured using a fluorescence microscope.

Western blot assay

Protein extracts from the collected nerve segments (1 cm of sciatic nerve spanning the injury site and the distal trunk), as well as the *in vitro* cultured nerve explants, were prepared by routine procedures, then separated on 10% dodecyl sulfate sodium salt-polyacrylamide gel electrophoresis gels and transferred to polyvinylidene fluoride membranes (Bio-Rad, Hercules, CA, USA). After blocking with 5% bovine serum albumin (GBCBIO, Guangzhou, China) in Tris-buffered solution containing 0.5% Tween-20 for 2 hours, the blots were probed overnight at 4°C with the following primary antibodies: rabbit anti-glyceraldehyde 3-phosphate dehydrogenase (1:3000, Cat# CW0101, Cwbiotech, Beijing, China), rabbit anti-tyrosinated (tyr)-tubulin (1:2000; Cat# MAB1864-I, Sigma), mouse anti-acetylated (ace)-tubulin (1:3000; Cat# T7451, Sigma), mouse anti-MBP (1:200; Cat# NE1018, Calbiochem, Darmstadt, Germany), rabbit anti-NF200 (1:1000, Cat# N0142, Sigma), rabbit anti-MAG (1:400; Cat# AB89780, Abcam), mouse anti-c-Jun (1:400; Cat# 610326, BD Biosciences), rabbit anti-GAP43 (1:1000; Cat# ab16053, Abcam), and rabbit anti-SCG10 (1:1000; Cat# NBP1–49461, Novusbio). Next, the blots were incubated with horseradish peroxidase-conjugated anti-rabbit secondary antibodies (1:2000, Cat# 65-6120, Molecular Probes) for 2 hours at room temperature, and were visualized using enhanced chemiluminescence (EpiZyme, Shanghai, China). Glyceraldehyde 3-phosphate dehydrogenase (GAPDH) was used as an internal reference. Finally, the density was calculated using Image-Pro Plus 6.0 software (Media Cybernetics). The relative protein expression levels were normalized to GAPDH.

Statistical analysis

All data are presented as mean ± standard error of the mean (SEM). All statistical analyses were performed with GraphPad Prism 5.0 software (GraphPad Software, San Diego, CA, USA) using one-way analysis of variance followed by Bonferroni's multiple test. A P value of < 0.05 was considered statistically significant.

Results

Effects of paclitaxel and nocodazole on microtubule dynamics

First we tested the effect of microtubule-targeting agents on microtubule stabilization and destabilization. Based on concentrations used in a previous report (Imai et al., 2017), we treated nerve explants with a series of concentrations of paclitaxel (0, 1, 10, 50, 100, or 200 nM) or nocodazole (0, 1, 10, 100, 500, or 1000 nM). As expected, expression of acetylated tubulin (ace-tub), a marker of stable microtubules (Xiong et al., 2019), was up-regulated with increasing paclitaxel concentrations, while expression of tyrosinated tubulin (tyr-tub), a marker of unstable microtubules (Hu et al., 2017), was down-regulated with increasing paclitaxel

concentrations. In contrast, treatment with nocodazole led to a decrease in ace-tub levels and an increase in tyr-tub levels (P < 0.05; **Figure 1A–F**).

Next, primary Schwann cells were isolated from neonatal rats, and passage 3 cells were treated with paclitaxel (1,10, 50, 100, or 200 nM) or nocodazole (1, 10, 100, 500, or 1000 nM) for 24 hours. As the drug concentration increased, the changes in cell morphology became more and more pronounced, and cell growth was increasingly hampered (**Figure 1G** & **H**). However, when the drugs were washed out, even the cells that had been treated with the highest concentrations recovered their normal morphology and regrew quickly (**Figure 1I** & **J**). These results indicate that the highest drug concentrations tested, 200 nM paclitaxel and 1000 nM nocodazole, safely regulate the microtubule dynamics of Schwann cells without inducing cell death; therefore, we chose these concentrations for use in subsequent experiments.

Effects of paclitaxel and nocodazole on axon and myelin degeneration

Nerve explant cultures have been demonstrated to be a reliable *in vitro* model for studying WD (Shin et al., 2014; Park et al., 2015; Li et al., 2021). This simplified model eliminates unpredictable factors that can interfere with *in vivo* experiments. The nerve explants were cultured for 5 or 8 days, after which longitudinal sections were stained with NF200 (an axonal marker (Hu et al., 2019)) and MBP (a myelin marker (Li et al., 2021)). The immunostaining results showed that both the axons and myelin were undergoing degeneration, which is characteristic of WD. We found that treatment with paclitaxel significantly accelerated axon and myelin degeneration, while treatment with nocodazole significantly inhibited this process (both P < 0.05; **Figure 2A–J**). Similar trends were observed when NF200 and MBP levels were assessed by western blot (P < 0.05; **Figure 2K–N**).

Effects of paclitaxel and nocodazole on myelin degeneration and fragmentation

ORO staining is used to label lipid droplets in adipocytes (Schachner-Nedherer et al., 2019; Velickovic et al., 2020). Recent studies have indicated that degenerated myelin fibers, which have a shrunken shape, also stain heavily with ORO, while normal myelin fibers, which have a circular shape, only stain faintly (Wang et al., 2020; Zou et al., 2020). Therefore, we stained cross sections of nerve explants cultured for 5 or 8 days with ORO and calculated the proportion of degenerated nerve fibers (shrunken myelin fibers with high fluorescence intensity) in each sample, as well as the mean intensity of ORO fluorescence. The proportion of degenerated myelin in the paclitaxel group was significantly higher than that in the vehicle group, and was the lowest in the nocodazole group (P < 0.05; **Figure 3**). Next, the nerves were teased into single nerve fibers and immunostained for α-tubulin to facilitate visualization of the myelin sheath by phase contrast microscopy. Myelin ovoids, which are the typical structure of a fragmented myelin sheath, was easily identified and quantified using this method (Jung et al., 2011) (**Figure 4A** and **B**). Consistent with the immunohistochemistry results, the number of myelin ovoids present in every 200-μm length of teased fiber (the ovoid index) (Jung et al., 2011) was highest in the paclitaxel group, followed by the vehicle group and then the nocodazole group (P < 0.05 among the three groups; **Figure 4C**).

Effects of paclitaxel and nocodazole on Schwann cell dedifferentiation

A WD progresses after PNI, mature Schwann cells undergo dedifferentiation. The dedifferentiated Schwann cells play a crucial role in WD; for example, they release chemoattractants to recruit macrophages that clear the debris of degenerated axons and myelin, and can phagocytose and degrade this debris themselves (Jang et al., 2017). Thus, we next performed immunostaining and western blotting with c-Jun (a marker of immature Schwann cells (Scapin et al., 2020)) and MAG (a marker of mature Schwann cells (Bolívar et al., 2020)) antibodies to evaluate Schwann cell dedifferentiation in nerve explants cultured for 5 or 8 days. The ratio of c-Jun/DAPI double-positive cells to all DAPI-positive cells and the level of c-Jun expression were dramatically higher in the cells induced with paclitaxel than in the vehicle and nocodazole groups, while both values were lowest in the nocodazole group. In contrast, the ratio of MAG/DAPI double-positive Schwann cells to all DAPI-positive Schwann cells and the level of MAG expression were significantly higher in the paclitaxel group than in the vehicle group, and both values were lowest in the nocodazole group (P < 0.05; **Figure 5**).

Effects of paclitaxel and nocodazole on nerve regeneration after sciatic nerve crush injury

To assess the role of microtubule dynamics on nerve regeneration, rats were subjected to sciatic nerve crush injury and immediately treated with paclitaxel, nocodazole, or saline (vehicle). Three days later, immunohistochemistry for GAP43 (a marker of axonal regeneration (Romeo-Guitart et al., 2020)) or SCG10 (a marker for regenerating sensory axons (Lai et al., 2020)) was performed on the injured nerves to detect regenerating axons. On cross sections taken 5 mm distal to the injured site, we found the highest density of both GAP43- and SCG10-positive axons in the paclitaxel group and the lowest density in the nocodazole group (P < 0.05; **Figure 6A–D**). To verify these results, total protein isolated from a 1-cm segment of the nerve spanning the injured site and the distal trunk was subjected to western blot. GAP43 and SCG10 expression in the injured nerve were significantly higher in the paclitaxel group compared with the vehicle group, and significantly lower in the nocodazole group (both P < 0.05; **Figure 6E–G**).

Based on our and others' previous studies, we selected 28 dpi as the time point for evaluating nerve recovery outcomes. At this time point, the numbers of NF200-positive axons and MBP/NF200 double positive myelinated axons in a cross section taken 5 mm distal to the injured site were highest in the paclitaxel group and lowest in the nocodazole group (P < 0.05; **Figure 7**). Next, we assessed the wet weight and total myofiber area of the gastrocnemius muscle, a key target muscle of the sciatic nerve, as these measures are widely used to assess nerve regeneration (Hu et al., 2020). Gross observation of the gastrocnemius muscles and closet observation of the hematoxylin-eosin-stained cross sections showed that myoatrophy was attenuated in the paclitaxel group compared with the vehicle group; however, myoatrophy was increased in the nocodazole group compared with the vehicle group (P < 0.05; **Figure 8**).

The ultimate aim of nerve repair is to restore nerve conduction and reverse functional losses (Wang et al., 2014; Li et al., 2019). SFI assessment is widely used to test the functional recovery of the injured hindlimb after sciatic nerve injury in animal models (Hu et al., 2020; de Oliveira Marques et al., 2021). Therefore, we performed this assessment using a footprint test system, and found that there was significantly greater motor function recovery in the paclitaxel group compared with the vehicle group, and significantly lower recovery in the nocodazole group (P < 0.05; **Figure 9A–C**). CMAP amplitude and latency can be evaluated to assess nerve conduction (Pan et al., 2017; Park et al., 2018) (**Figure 9D**). Statistical analysis of the CMAP images generated in our study showed that, compared with the vehicle group, treatment with paclitaxel resulted in a higher amplitude (which indicates that more axons regenerated and arrived at the muscles measured in the paws (Zhan et al., 2013)), as well as a shorter latency (which corresponds to quicker nerve conduction (Pan et al., 2017)). The nocodazole group exhibited the lowest amplitude and longest latency among all three groups (P < 0.05; **Figure 9E** & **F**).

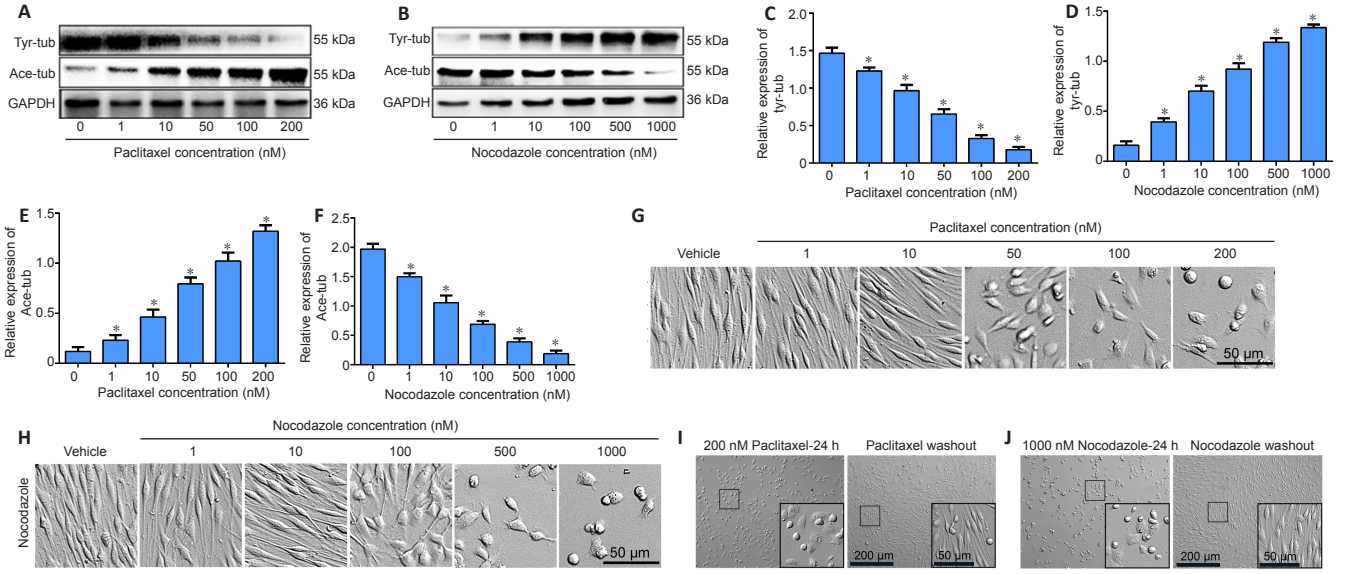

Figure 1 | **The effects of paclitaxel and nocodazole on microtubule dynamics in nerve explant Schwann cells.**
(A, B) Western blot showing ace-tub and tyr-tub expression after exposure to paclitaxel or nocodazole. (C–F) Relative expression of tyr-tub (C, D) and ace-tub (E, F), normalized with GAPDH. (G, H) Phase contrast microscopy images showing the morphologic changes in primary cultured Schwann cells after exposure to different concentrations of paclitaxel or nocodazole for 24 hours. When the Schwann cells were exposed to 50 nM paclitaxel or 100 nM nocordazole, they began to show morphologic changes, including retraction of protrusions, cell body hypertrophy, and rounding. As the drug concentration increased, the deformation intensified. (I, J) Images showing that the morphologic changes induced by paclitaxel or nocodazole treatment could be reversed by drug washout. Scale bars: 50 μm in G and H, 200 μm in I and J, and 50 μm in the enlarged parts of I and J. Data are expressed as the mean ± SEM (n = 3 per group). *P < 0.05, *vs.* the control group (one-way analysis of variance followed by Bonferroni's multiple test). ace-tub: Acetylated tubulin; GAPDH: glyceraldehyde 3-phosphate dehydrogenase; tyr-tub: tyrosinated tubulin.

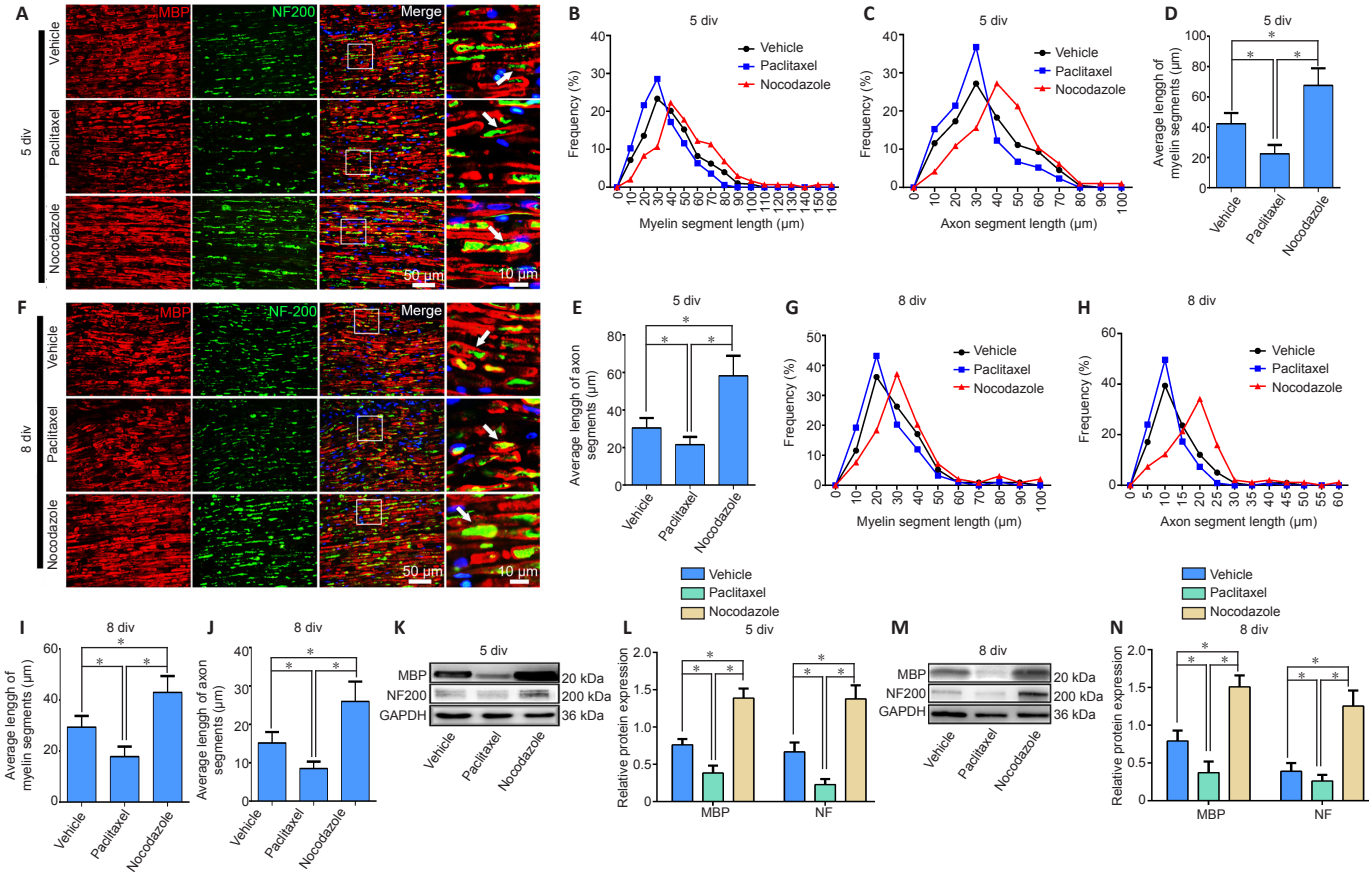

Figure 2 | **Paclitaxel and nocodazole affect axon and myelin degeneration in nerve explants.**
(A) Immunohistochemistry images showing fragmented axons (NF200, red, stained with Alexa Fluor 568) and myelin sheaths (MBP, green, stained with Alexa Fluor 488) (white arrows) in longitudinal sections of sciatic nerve explants treated with paclitaxel or nocodazole at 5 or 8 div. The number of fragments in five 100 μm × 100 μm fields (the middle of the nerve and the four quadrants) was quantified. The axon and myelin fragment lengths were significantly shorter in the paclitaxel group than in the vehicle and nocodazole groups. Scale bars: 50 μm, 10 μm in the enlarged parts. (B–E) Length distribution of axons and myelin fragments at 5 div. (F) Immunohistochemistry images showing the fragmented axons and myelin sheaths in longitudinal sections of sciatic nerve explants treated with paclitaxel or nocodazole at 8 div. The differences among the three groups were similar to those seen at 5 div. (G–J) Length distribution of axons and myelin fragments at 8 div. (K, L) Western blot analysis of MBP and NF200 expression levels at 5 div. (M, N) Western blot showing MBP and NF200 expression levels at 8 div. MBP and NF200 expression was normalized to GAPDH. Data are expressed as the mean ± SEM (n = 3 per group). *P < 0.05 (one-way analysis of variance followed by Bonferroni's multiple test). DAPI: 4′,6-Diamidino-2-phenylindole; div: days *in vitro*; GAPDH: glyceraldehyde 3-phosphate dehydrogenase; MBP: myelin basic protein; NF200: neurofilament 200.

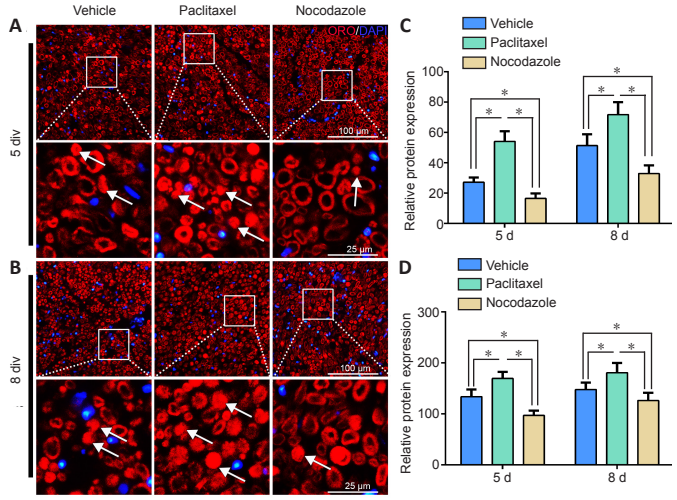

Figure 3 | The effects of paclitaxel and nocodazole on myelin degeneration in nerve explants.

(A, B) ORO staining showed that myelin sheath degeneration (shrunken myelin with high fluorescence intensity, indicated by white arrows) appeared in nerve explants at 5 and 8 div. The paclitaxel group exhibited the highest ratio of degenerated myelin sheaths to all myelin sheaths and fluorescence intensity among the three groups. Scale bars: 100 μm, 25 μm in the enlarged parts. (C, D) Ratio of degenerative myelin and mean fluorescence intensity quantification, respectively, in a 200 μm × 200 μm area. Data are expressed as the mean ± SEM (n = 3 per group). *P < 0.05 (one-way analysis of variance followed by Bonferroni's multiple test). DAPI: 4′,6-Diamidino-2-phenylindole; div: days *in vitro*; ORO: oil red O.

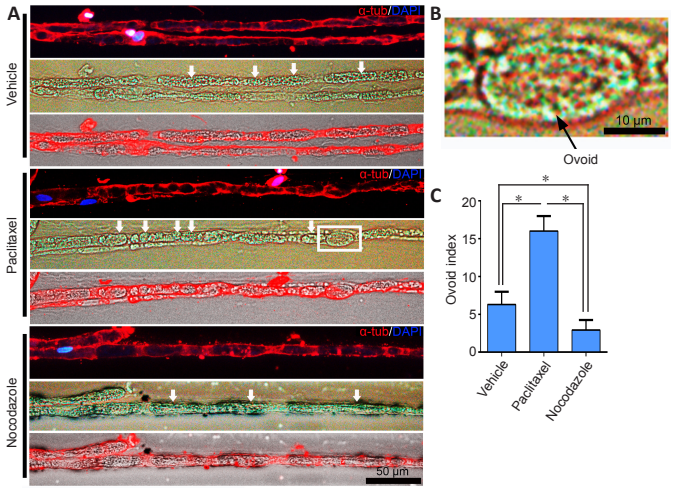

Figure 4 | Teased nerve explant fibers exhibit myelin ovoid formation.

(A) Teased fibers from sciatic nerve explants (5 div) treated with paclitaxel or nocodazole were stained with an anti-α-tub antibody (red, Alexa Fluor 568) (upper). The phase contrast images (middle) show the myelin ovoids (arrows). The bottom images are merged fluorescence and phase contrast images. The paclitaxel group exhibited the most myelin ovoids among the three groups. Scale bar: 50 μm. (B) An enlarged image from the paclitaxel group showing the ovoid (arrow) clearly. (C) Ovoid index. Data are expressed as the mean ± SEM (n = 3 per group). *P < 0.05 (one-way analysis of variance followed by Bonferroni's multiple test). α-tub: α-Tubulin; DAPI: 4′,6-diamidino-2-phenylindole; div: days *in vitro*.

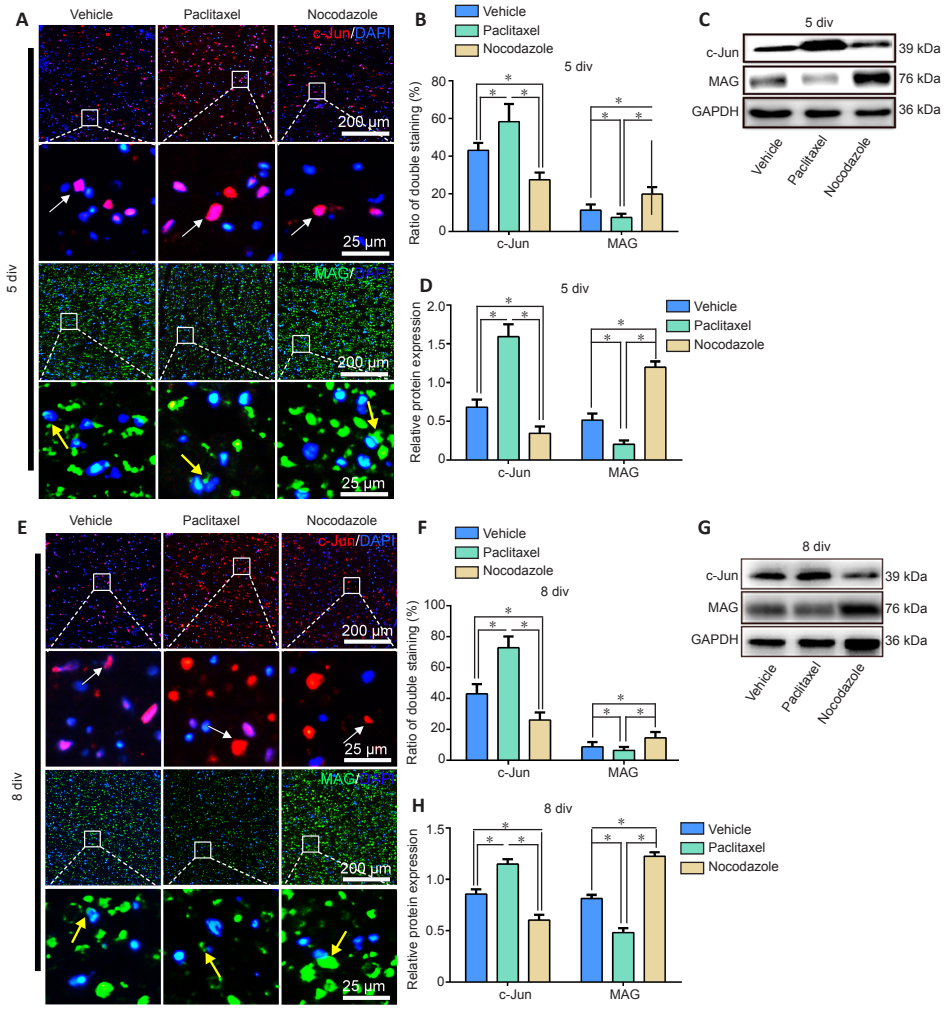

Figure 5 | Effects of paclitaxel and nocodazole on Schwann cell dedifferentiation in sciatic nerve explants.

(A) Immunofluorescence images of c-Jun- (red, Alexa Fluor 568) (white arrows) and MAG- (green, Alexa Fluor 488) (yellow arrows) positive Schwann cells in sciatic nerve explants at 5 div. The ratio of c-Jun/DAPI double-positive Schwann cells to total cells in the paclitaxel group was higher than in the vehicle and nocodazole groups, and the ratio of MAG/DAPI double-positive Schwann cells to all DAPI-positive Schwann cells was lowest in the paclitaxel group among the three groups. Scale bars: 200 μm (25 μm in the enlarged parts). (B) The number of c-Jun- or MAG-positive Schwann cells in a 500 μm × 500 μm area at 5 div. (C, D) Western blot analysis of c-Jun and MAG expression levels in sciatic nerve explants at 5 div. (E) Immunofluorescence staining showing c-Jun- and MAG-positive Schwann cells at 8 div. The differences among the three groups are similar to those seen at 8 div. Scale bars: 200 μm, 25 μm in the enlarged parts. (F) The number of c-Jun- or MAG-positive Schwann cells at 8 div. (G, H) Western blot analysis of c-Jun and MAG expression levels in sciatic nerve explants at 8 div. c-Jun and MAG expression levels were normalized to GAPDH. Data are expressed as the mean ± SEM (n = 3 per group). *P < 0.05 (one-way analysis of variance followed by Bonferroni's multiple test). DAPI: 4′,6-Diamidino-2-phenylindole; div: days *in vitro*; GAPDH: glyceraldehyde 3-phosphate dehydrogenase; MAG: myelin-associated glycoprotein.

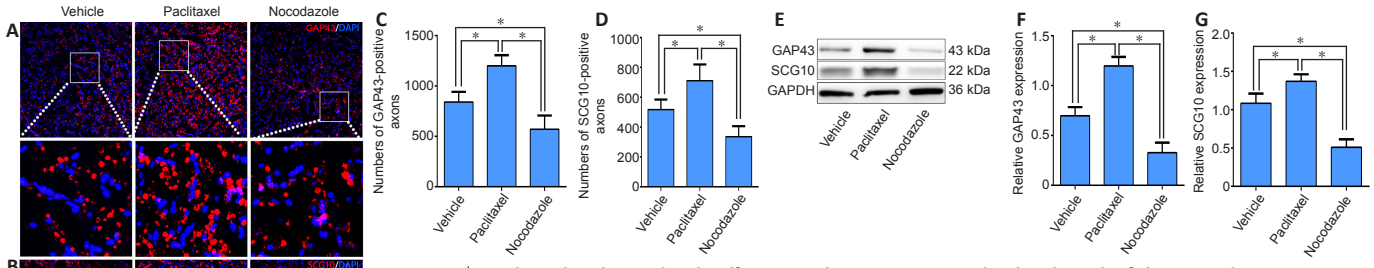

Figure 6 | Paclitaxel and nocodazole affect axonal regeneration in the distal trunk of the injured sciatic nerve at 3 dpi.

(A, B) Immunostaining showing GAP43- (red, Alexa Fluor 568) and SCG10- (red, Alexa Fluor 568) positive axons in cross sections of sciatic nerves 5 mm distal to the injury site. The number of GAP43- or SCG10-positive axons was markedly higher in the paclitaxel group than in vehicle and nocodazole groups, and was lowest in the nocodazole group. Scale bars: 200 μm, 50 μm in the enlarged parts. (C, D) The number of GAP43- or SCG10-positive axons in a 800 μm × 800 μm area. (E–G) Western blot analysis of GAP43 and SCG10 expression levels in the distal trunk of the injured nerve (1-cm segment spanning the injury site and the distal trunk). GAP43 and SCG10 expression levels were normalized to GAPDH. Data are expressed as the mean ± SEM (n = 3 per group). *P < 0.05 (one-way analysis of variance followed by Bonferroni's multiple test). DAPI: 4′,6-Diamidino-2-phenylindole; dpi: days post-injury; GAPDH: glyceraldehyde 3-phosphate dehydrogenase; GAP43: growth-associated protein 43; SCG10: superior cervical ganglia protein 10.

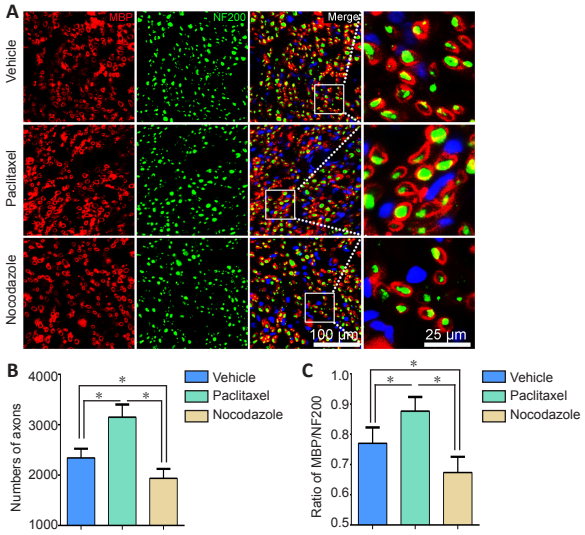

Figure 7 | Effects of paclitaxel and nocodazole on nerve regeneration of the injured sciatic nerve at 28 dpi.

(A) Cross sections of the sciatic nerve immunostained with NF200 (green, Alexa Fluor 488) and MBP (red, Alexa Fluor 568) showing regenerated and remyelinated axons in the control, paclitaxel, and nocodazole groups, respectively. Compared with the control group, the number of NF200-positive axons (with diameter > 1 μm) was dramatically higher in the paclitaxel group and dramatically lower in the nocodazole group, and the ratio of MBP/NF200 double-positive nerve fibers to all NF200-positive axons (with diameter > 1 μm) in the paclitaxel group was greater than that in the vehicle and nocodazole groups, and lowest in the nocodazole group. Scale bars: 100 μm, 25 μm in the enlarged parts. (B, C) The number of NF-positive axons and the MBP/NF ratio from each group an 800 μm × 800 μm area of nerve cross sections. Data are expressed as the mean ± SEM (n = 3 per group). *P < 0.05 (one-way analysis of variance followed by Bonferroni's multiple test). DAPI: 4′,6-Diamidino-2-phenylindole; dpi: days post-injury; MBP: myelin basic protein; NF200: neurofilament 200.

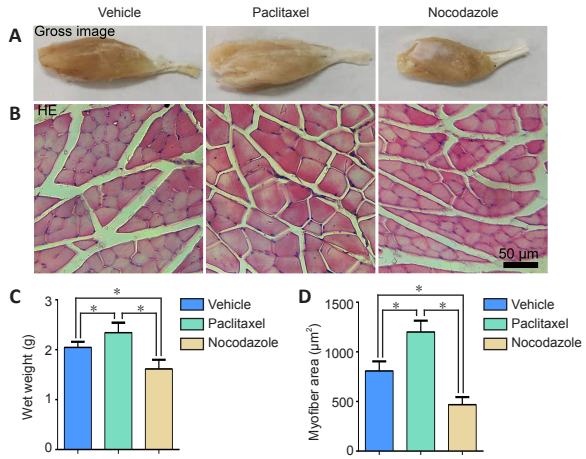

Figure 8 | Effects of paclitaxel and nocodazole on gastrocnemius muscle myoatrophy in rats with sciatic nerve injury.

(A) Representative gross images of the gastrocnemius muscle in each group. There was less myoatrophy in the paclitaxel group compared with the vehicle group, while the nocodazole group showed the greatest degree of myoatrophy. (B) HE-stained transverse sections of muscles from each group collected at 28 dpi. The size of the myofibers in the gastrocnemius muscles was significantly greater in the paclitaxel group compared with the control group, and markedly smaller in the nocodazole group. Scale bar: 50 μm. (C, D) Gastrocnemius muscle wet weight and total myofiber area in each group. Data are expressed as the mean ± SEM (n = 3 per group). *P < 0.05 (one-way analysis of variance followed by Bonferroni's multiple test). dpi: days post-injury; HE: hematoxylin-eosin.

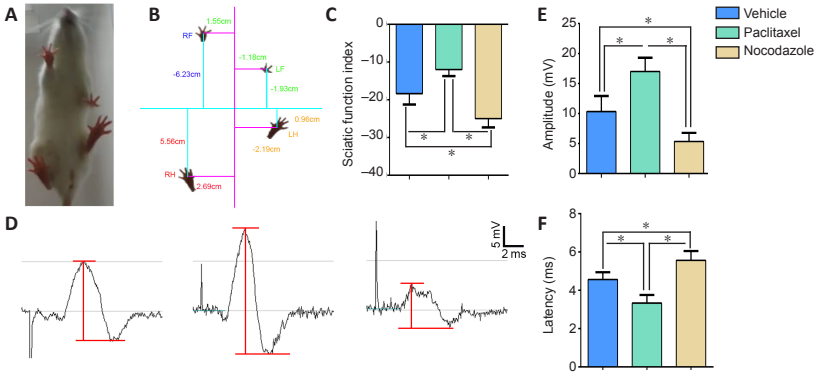

Figure 9 | Effects of paclitaxel and nocodazole on functional recovery after sciatic nerve injury.

(A, B) An example and schematic of the gait analysis at 28 days post-injury. (C) Quantification of the sciatic function index. (D) Respective images of the compound muscle action potential (red lines) in the control, paclitaxel, and nocodazole groups. (E, F) Quantification of compound muscle action potential amplitude and latency. Data are expressed as the mean ± SEM (n = 3 per group). *P < 0.05 (one-way analysis of variance followed by Bonferroni's multiple test). LF: Left forefoot; LH: left hindfoot; RF: right forefoot; RH: right hindfoot.

Discussion

It is well-known that microtubules play pivotal roles in most cellular activities, and that microtubule dynamics are crucial to their function (Zhang et al., 2015; Fedorov et al., 2019). Microtubule-targeting agents are used in the treatment of various diseases to stabilize or destabilize microtubules for therapeutic effect (Kaul et al., 2019; Peronne et al., 2020). To date, however, there have been no reports of the role of microtubule dynamics in WD after PNI. This study demonstrates, for the first time, that paclitaxel and nocodazole treatment can accelerate and attenuate demyelination and Schwann cell dedifferentiation during WD, respectively, and suggests that altering microtubule dynamics has a profound impact on WD. Indeed, earlier studies have shown that paclitaxel treatment results in a higher frequency of dysmyelination or demyelination in untreated sciatic nerves (Benbow et al., 2016; Cook et al., 2018), disrupts myelin formation in Schwann cell/dorsal root ganglion neuron co-cultures, and leads to dedifferentiation of Schwann cells (Imai et al., 2017). Consistent with these studies, we also found that paclitaxel promotes demyelination and dedifferentiation. Taken together with the existing literature, our findings indicate that paclitaxel-induced microtubule stability promotes WD, while nocodazole-induced microtubule instability inhibits WD.

Many studies have shown that paclitaxel promotes axonal regeneration after central nervous system injury (Hellal et al., 2011; Sengottuvel et al., 2011; Austin et al., 2017). In addition, epothilone B, another microtubule-stabilizing agent, facilitates peripheral nerve regeneration (Zhou et al., 2020). Similar to these earlier studies, the present study illustrates that paclitaxel treatment significantly enhances morphologic and functional recovery in the injured sciatic nerve and its target muscles. However, the results reported by Hsu et al. (2017) suggest that paclitaxel inhibits peripheral nerve regeneration. To address this apparent controversy, in the present study we assessed the effects not only of paclitaxel, but also of nocodazole, which has the opposite effect in that it promotes microtubule destabilization (Endo et al., 2020; Marquis et al., 2021). As expected, nocodazole treatment not only inhibited WD but also attenuated post-PNI morphologic and functional regeneration. WD is essential for nerve regeneration, as the debris of degenerated axons and myelin needs to be cleaned up as quickly as possible to create a favorable microenvironment for promoting subsequent nerve regeneration (Bombeiro et al., 2020). Although the deeper underlying mechanisms require further investigation, the results from the present study suggest that microtubule stabilization may be conducive to peripheral nerve regeneration, due at least in part to the role of this process in WD.

In summary, the current study used an *in vitro* nerve explant model and an *in vivo* rat model of sciatic nerve crush injury to show that paclitaxel-induced microtubule stabilization promotes WD and facilitates structural and functional recovery after PNI. In contrast, nocodazole-induced microtubule destabilization has the opposite effect. Regarding the limitations of this study, there was no inherent bias, but the underlying mechanisms of how microtubule dynamics regulate WD have yet to be elucidated.

Author contributions: *Study conception and design: JG; animal surgery: JL, LL, YX; immunohistochemistry: JL, LF, JZ, ML; western blot assay: JL, YZ, HZ, XH; Schwann cells culture: JL, XM, JX; behavioral assessment and electrophysiological test: JL, XW, ZL; histomorphometry of the gastrocnemius muscle: JL, data analysis: JL, HS, HZ, LZ; manuscript writing: JL, JG. All authors approved the final version of the manuscript.*

Conflicts of interest: *The authors declare no conflict of interest.*

Financial support: *This work was supported by the National Natural Science Foundation of China, Nos. 82071386 (to JS), 81870982 (to JS) & 81571182 (to JS); National Key Basic Research Program of China, No. 2014CB542202 (to JS); the Program for Changjiang Scholars and Innovative Research Team in University of China, No. IRT-16R37 (to JS); Key Research & Development Program of Guangzhou Regenerative Medicine and Health Guangdong Laboratory of China, No. 2018GZR110104008 (to HZ); Research Grant of Guangdong Province Key Laboratory of Psychiatric Disorders of China, No. N201904 (to JS); and Natural Science Foundation of Guangdong Province of China, No. 2017A030312009 (to JS). The funding sources had no role in study conception and design, data analysis or interpretation, paper writing or deciding to submit this paper for publication.*

Institutional review board statement: *This study was approved by the Southern Medical University Animal Care and Use Committee (approval No. SMU-L2015081) on October 15, 2015.*

Data sharing statement: *Datasets analyzed during the current study are available from the corresponding author on reasonable request.*

Plagiarism check: *Checked twice by iThenticate.*

Peer review: *Externally peer reviewed.*

Open peer reviewer: *Kathryn R Moss, Johns Hopkins Medicine, USA.*

Additional files:

Additional Figure 1: *The experiment process.*

Additional file 1: *Open peer review report 1.*

References

Austin TO, Matamoros AJ, Friedman JM, Friedman AJ, Nacharaju P, Yu W, Sharp DJ, Baas PW (2017) Nanoparticle delivery of fidgetin siRNA as a microtubule-based therapy to augment nerve regeneration. Sci Rep 7:9675.

Benbow SJ, Cook BM, Reifert J, Wozniak KM, Slusher BS, Littlefield BA, Wilson L, Jordan MA, Feinstein SC (2016) Effects of paclitaxel and eribulin in mouse sciatic nerve: a microtubule-based rationale for the differential induction of chemotherapy-induced peripheral neuropathy. Neurotox Res 29:299-313.

Bolívar S, Navarro X, Udina E (2020) Schwann cell role in selectivity of nerve regeneration. Cells 9:2131.

Bombeiro AL, Lima BHM, Bonfanti AP, Oliveira ALR (2020) Improved mouse sciatic nerve regeneration following lymphocyte cell therapy. Mol Immunol 121:81-91.

Conforti L, Gilley J, Coleman MP (2014) Wallerian degeneration: an emerging axon death pathway linking injury and disease. Nat Rev Neurosci 15:394-409.

Cook BM, Wozniak KM, Proctor DA, Bromberg RB, Wu Y, Slusher BS, Littlefield BA, Jordan MA, Wilson L, Feinstein SC (2018) Differential morphological and biochemical recovery from chemotherapy-induced peripheral neuropathy following paclitaxel, ixabepilone, or eribulin treatment in mouse sciatic nerves. Neurotox Res 34:677-692.

de Oliveira Marques C, Amaro Espindula I, Kwame Karikari Darko E, Viçosa Bonetti L, Sonza A, Aparecida Partata W, Faccioni-Heuser MC, Malysz T (2021) Whole-body vibration therapy does not improve the peripheral nerve regeneration in experimental model. J Musculoskelet Neuronal Interact 21:68-78.

Endo Y, Saeki K, Watanabe M, Miyajima-Magara N, Igarashi M, Mochizuki M, Nishimura R, Sugano S, Sasaki N, Nakagawa T (2020) Spindle assembly checkpoint competence in aneuploid canine malignant melanoma cell lines. Tissue Cell 67:101403.

Fedorov VA, Orekhov PS, Kholina EG, Zhmurov AA, Ataullakhanov FI, Kovalenko IB, Gudimchuk NB (2019) Mechanical properties of tubulin intra- and inter-dimer interfaces and their implications for microtubule dynamic instability. PLoS Comput Biol 15:e1007327.

Fees CP, Moore JK (2018) Regulation of microtubule dynamic instability by the carboxy-terminal tail of β-tubulin. Life Sci Alliance 1:e201800054.

Felitsyn N, Stacpoole PW, Notterpek L (2007) Dichloroacetate causes reversible demyelination in vitro: potential mechanism for its neuropathic effect. J Neurochem 100:429-436.

Glajch KE, Fleming SM, Surmeier DJ, Osten P (2012) Sensorimotor assessment of the unilateral 6-hydroxydopamine mouse model of Parkinson's disease. Behav Brain Res 230:309-316.

Guo J, Wang L, Zhang Y, Wu J, Arpag S, Hu B, Imhof BA, Tian X, Carter BD, Suter U, Li J (2014) Abnormal junctions and permeability of myelin in PMP22-deficient nerves. Ann Neurol 75:255-265.

Hellal F, Hurtado A, Ruschel J, Flynn KC, Laskowski CJ, Umlauf M, Kapitein LC, Strikis D, Lemmon V, Bixby J, Hoogenraad CC, Bradke F (2011) Microtubule stabilization reduces scarring and causes axon regeneration after spinal cord injury. Science 331:928-931.
Honoré S, Hubert F, Tournus M, White D (2019) A growth-fragmentation approach for modeling microtubule dynamic instability. Bull Math Biol 81:722-758.
Hsu ST, Yao CH, Hsu YM, Lin JH, Chen YH, Chen YS (2017) Effects of taxol on regeneration in a rat sciatic nerve transection model. Sci Rep 7:42280.
Hu BB, Chen M, Huang RC, Huang YB, Xu Y, Yin W, Li L, Hu B (2018) In vivo imaging of Mauthner axon regeneration, remyelination and synapses re-establishment after laser axotomy in zebrafish larvae. Exp Neurol 300:67-73.
Hu ML, Zhang WW, Cao H, Zhang YQ (2019) Expression pattern of type 3 adenylyl cyclase in rodent dorsal root ganglion and its primary afferent terminals. Neurosci Lett 692:16-22.
Hu X, Wang X, Xu Y, Li L, Liu J, He Y, Zou Y, Yu L, Qiu X, Guo J (2020) Electric conductivity on aligned nanofibers facilitates the transdifferentiation of mesenchymal stem cells into Schwann cells and regeneration of injured peripheral nerve. Adv Healthc Mater 9:e1901570.
Hu Z, Feng J, Bo W, Wu R, Dong Z, Liu Y, Qiang L, Liu M (2017) Fidgetin regulates cultured astrocyte migration by severing tyrosinated microtubules at the leading edge. Mol Biol Cell 28:545-553.
Imai S, Koyanagi M, Azimi Z, Nakazato Y, Matsumoto M, Ogihara T, Yonezawa A, Omura T, Nakagawa S, Wakatsuki S, Araki T, Kaneko S, Nakagawa T, Matsubara K (2017) Taxanes and platinum derivatives impair Schwann cells via distinct mechanisms. Sci Rep 7:5947.
Jang SY, Yoon BA, Shin YK, Yun SH, Jo YR, Choi YY, Ahn M, Shin T, Park JI, Kim JK, Park HT (2017) Schwann cell dedifferentiation-associated demyelination leads to exocytotic myelin clearance in inflammatory segmental demyelination. Glia 65:1848-1862.
Jung J, Cai W, Lee HK, Pellegatta M, Shin YK, Jang SY, Suh DJ, Wrabetz L, Feltri ML, Park HT (2011) Actin polymerization is essential for myelin sheath fragmentation during Wallerian degeneration. J Neurosci 31:2009-2015.
Kaul R, Risinger AL, Mooberry SL (2019) Microtubule-targeting drugs: more than antimitotics. J Nat Prod 82:680-685.
Lai M, Pan M, Ge L, Liu J, Deng J, Wang X, Li L, Wen J, Tan D, Zhang H, Hu X, Fu L, Xu Y, Li Z, Qiu X, Chen G, Guo J (2020) NeuroD1 overexpression in spinal neurons accelerates axonal regeneration after sciatic nerve injury. Exp Neurol 327:113215.
Li L, Xu Y, Wang X, Liu J, Hu X, Tan D, Li Z, Guo J (2021) Ascorbic acid accelerates Wallerian degeneration after peripheral nerve injury. Neural Regen Res 16:1078-1085.
Li L, Li Y, Fan Z, Wang X, Li Z, Wen J, Deng J, Tan D, Pan M, Hu X, Zhang H, Lai M, Guo J (2019) Ascorbic acid facilitates neural regeneration after sciatic nerve crush injury. Front Cell Neurosci 13:108.
Maciel R, Bis DM, Rebelo AP, Saghira C, Züchner S, Saporta MA (2018) The human motor neuron axonal transcriptome is enriched for transcripts related to mitochondrial function and microtubule-based axonal transport. Exp Neurol 307:155-163.
Manka SW, Moores CA (2018) The role of tubulin-tubulin lattice contacts in the mechanism of microtubule dynamic instability. Nat Struct Mol Biol 25:607-615.
Marquis C, Fonseca CL, Queen KA, Wood L, Vandal SE, Malaby HLH, Clayton JE, Stumpff J (2021) Chromosomally unstable tumor cells specifically require KIF18A for proliferation. Nat Commun 12:1213.
Nocera G, Jacob C (2020) Mechanisms of Schwann cell plasticity involved in peripheral nerve repair after injury. Cell Mol Life Sci 77:3977-3989.
Pan M, Wang X, Chen Y, Cao S, Wen J, Wu G, Li Y, Li L, Qian C, Qin Z, Li Z, Tan D, Fan Z, Wu W, Guo J (2017) Tissue engineering with peripheral blood-derived mesenchymal stem cells promotes the regeneration of injured peripheral nerves. Exp Neurol 292:92-101.
Park BS, Kim HW, Rhyu IJ, Park C, Yeo SG, Huh Y, Jeong NY, Jung J (2015) Hydrogen sulfide is essential for Schwann cell responses to peripheral nerve injury. J Neurochem 132:230-242.
Park HJ, Shin HY, Kim SH, Jeong HN, Choi YC, Suh BC, Park KD, Kim SM (2018) Partial conduction block as an early nerve conduction finding in neurolymphomatosis. J Clin Neurol 14:73-80.
Peronne L, Denarier E, Rai A, Prudent R, Vernet A, Suzanne P, Ramirez-Rios S, Michallet S, Guidetti M, Vollaire J, Lucena-Agell D, Ribba AS, Josserand V, Coll JL, Dallemagne P, Díaz JF, Oliva M, Sadoul K, Akhmanova A, Andrieux A, et al. (2020) Two antagonistic microtubule targeting drugs act synergistically to kill cancer cells. Cancers (Basel) 12:2196.
Qian C, Tan D, Wang X, Li L, Wen J, Pan M, Li Y, Wu W, Guo J (2018) Peripheral nerve injury-induced astrocyte activation in spinal ventral horn contributes to nerve regeneration. Neural Plast 2018:8561704.
Qu WR, Zhu Z, Liu J, Song DB, Tian H, Chen BP, Li R, Deng LX (2021) Interaction between Schwann cells and other cells during repair of peripheral nerve injury. Neural Regen Res 16:93-98.
Romeo-Guitart D, Leiva-Rodríguez T, Casas C (2020) SIRT2 inhibition improves functional motor recovery after peripheral nerve injury. Neurotherapeutics 17:1197-1211.
Roviello G, Conter FU, Mini E, Generali D, Traversini M, Lavacchi D, Nobili S, Sobhani N (2019) Nanoparticle albumin-bound paclitaxel: a big nano for the treatment of gastric cancer. Cancer Chemother Pharmacol 84:669-677.
Scapin C, Ferri C, Pettinato E, Bianchi F, Del Carro U, Feltri ML, Kaufman RJ, Wrabetz L, D'Antonio M (2020) Phosphorylation of eIF2α promotes schwann cell differentiation and myelination in CMT1B mice with activated UPR. J Neurosci 40:8174-8187.
Schachner-Nedherer AL, Werzer O, Kornmueller K, Prassl R, Zimmer A (2019) Biological activity Of miRNA-27a using peptide-based drug delivery systems. Int J Nanomedicine 14:7795-7808.
Senese S, Lo YC, Gholkar AA, Li CM, Huang Y, Mottahedeh J, Kornblum HI, Damoiseaux R, Torres JZ (2017) Microtubins: a novel class of small synthetic microtubule targeting drugs that inhibit cancer cell proliferation. Oncotarget 8:104007-104021.
Sengottuvel V, Leibinger M, Pfreimer M, Andreadaki A, Fischer D (2011) Taxol facilitates axon regeneration in the mature CNS. J Neurosci 31:2688-2699.
Shin YH, Lee SJ, Jung J (2013) Extracellular ATP inhibits Schwann cell dedifferentiation and proliferation in an ex vivo model of Wallerian degeneration. Biochem Biophys Res Commun 430:852-857.
Shin YH, Chung HJ, Park C, Jung J, Jeong NY (2014) Adenosine 5'-triphosphate (ATP) inhibits Schwann cell demyelination during Wallerian degeneration. Cell Mol Neurobiol 34:361-368.
Tan D, Wen J, Li L, Wang X, Qian C, Pan M, Lai M, Deng J, Hu X, Zhang H, Guo J (2018) Inhibition of RhoA-subfamily GTPases suppresses Schwann cell proliferation through regulating AKT pathway rather than ROCK pathway. Front Cell Neurosci 12:437.
Triolo D, Dina G, Taveggia C, Vaccari I, Porrello E, Rivellini C, Domi T, La Marca R, Cerri F, Bolino A, Quattrini A, Previtali SC (2012) Vimentin regulates peripheral nerve myelination. Development 139:1359-1367.
Velickovic K, Lugo Leija HA, Surrati A, Kim DH, Sacks H, Symonds ME, Sottile V (2020) Targeting glutamine synthesis inhibits stem cell adipogenesis in vitro. Cell Physiol Biochem 54:917-927.
Wang SS, Bi HZ, Chu SF, Dong YX, He WB, Tian YJ, Zang YD, Zhang DM, Zhang Z, Chen NH (2020) CZ-7, a new derivative of Claulansine F, promotes remyelination induced by cuprizone by enhancing myelin debris clearance. Brain Res Bull 159:67-78.
Wang X, Pan M, Wen J, Tang Y, Hamilton AD, Li Y, Qian C, Liu Z, Wu W, Guo J (2014) A novel artificial nerve graft for repairing long-distance sciatic nerve defects: a self-assembling peptide nanofiber scaffold-containing poly(lactic-co-glycolic acid) conduit. Neural Regen Res 9:2132-2141.
Wang Y, Shan Q, Pan J, Yi S (2018) Actin cytoskeleton affects schwann cell migration and peripheral nerve regeneration. Front Physiol 9:23.
Wen J, Tan D, Li L, Wang X, Pan M, Guo J (2018) RhoA regulates Schwann cell differentiation through JNK pathway. Exp Neurol 308:26-34.
Wen J, Qian C, Pan M, Wang X, Li Y, Lu Y, Zhou Z, Yan Q, Li L, Liu Z, Wu W, Guo J (2017) Lentivirus-mediated RNA interference targeting RhoA slacks the migration, proliferation, and myelin formation of Schwann cells. Mol Neurobiol 54:1229-1239.
Wu RH, Wang P, Yang L, Li Y, Liu Y, Liu M (2011) A potential indicator of denervated muscle atrophy: the ratio of myostatin to follistatin in peripheral blood. Genet Mol Res 10:3914-3923.
Xiong TQ, Guo CY, Tan BH, Gui Y, Li YC (2019) The temporal and spatial changes of microtubule cytoskeleton in the CA1 stratum radiatum following global transient ischemia. J Chem Neuroanat 101:101682.
Zhan X, Gao M, Jiang Y, Zhang W, Wong WM, Yuan Q, Su H, Kang X, Dai X, Zhang W, Guo J, Wu W (2013) Nanofiber scaffolds facilitate functional regeneration of peripheral nerve injury. Nanomedicine 9:305-315.
Zhang R, Alushin GM, Brown A, Nogales E (2015) Mechanistic origin of microtubule dynamic instability and its modulation by EB proteins. Cell 162:849-859.
Zhou J, Li S, Gao J, Hu Y, Chen S, Luo X, Zhang H, Luo Z, Huang J (2020) Epothilone B facilitates peripheral nerve regeneration by promoting autophagy and migration in schwann cells. Front Cell Neurosci 14:143.
Zou Z, Sun J, Kang Z, Wang Y, Zhao H, Zhu K, Wang J (2020) Tyrosine kinase receptors Axl and MerTK mediate the beneficial effect of electroacupuncture in a cuprizone-induced demyelinating model. Evid Based Complement Alternat Med 2020:3205176.

P-Reviewer: Moss KR; C-Editor: Zhao M; S-Editors: Yu J, Li CH; L-Editors: Crow E, Yu J, Song LP; T-Editor: Jia Y

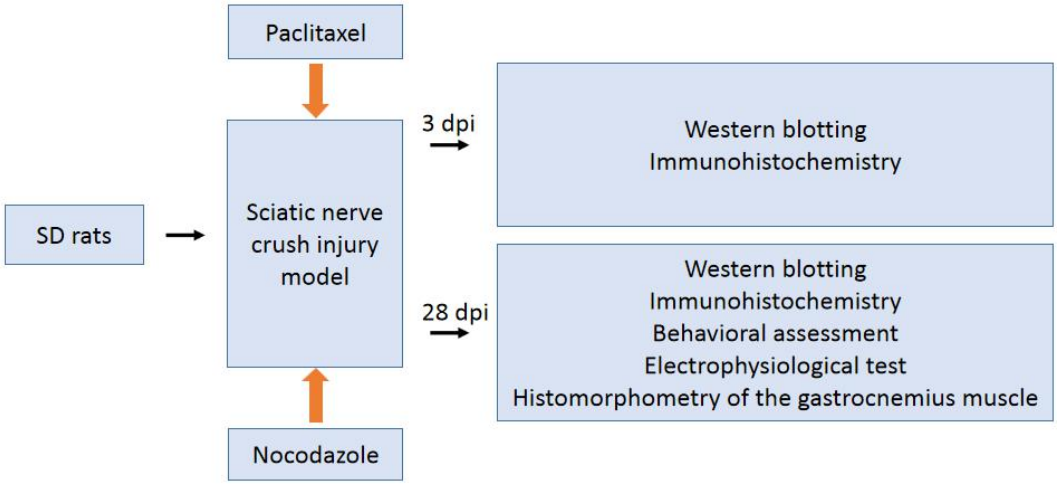

Additional Figure 1 The experiment process.

dpi: Days post injury; SD: Sprague-Dawley.